NUMERICAL INVESTIGATION ON COOLING RATE IN PROTON EXCHANGE MEMBRANE FUEL CELL USING PROPYLENE GLYCOL FLUID

by

Dillip Kumar SAHOO**, Gowtham Sri RAM, and Sriram PRASATH

School of Mechanical Engineering,
Sathyabama Institute of Science and Technology, Chennai, Tamil Nadu, India

Original scientific paper
https://doi.org/10.2298/TSCI220429040S

In this study, a cooling channel was constructed inside the fuel cell to examine the impact of cooling on proton exchange membrane fuel cell performance. The performance of the fuel cell was assessed using four different coolant mixtures: DI100 (100% deionized water – DI), PG10 (90% DI water + 10% propylene glycol), PG20 (80% DI water + 20% propylene glycol), and PG30 (70% DI water + 30% propylene glycol). The efficiency of the fuel cell, system temperature, operating parameters, coolant, and cooling channel shape of the fuel cell were tested using a CFD model based on the finite volume approach. The test results showed that the fuel cell performance was good for both single-cell fuel cells and fuel cell stacks at temperatures of 354 K and 360 K, respectively. However, as the membrane became dehydrated above 362 K for single cell fuel cells and after 371 K for fuel cell stacks, performance of the fuel cell decreased and no appreciable improvement was seen. For single cells, the fuel cell showed good performance improvement at PG30 combinations, whereas the best performance in stacks was attained at PG20 combinations.

Key words: *proton exchange membrane fuel cell, deionized water, propylene glycol, cooling system, cooling additives*

Introduction

Despite recent advancements in the polymeric fuel cell's performance, appropriate heat control remains a fundamental challenge. Heat management in the cell is defined as the dispersion or transfer of produced heat to nature from inside the cell mass [1]. The heat generated by electrochemical processes, reaction inevitability, and the fluid-phase transition is critical components of heat generation in the cell [2]. In other words, while some cells have higher energy efficiency (about 40-50%), they also release a large amount of heat, which is approximately equal to, if not somewhat more significant than, the electrical energy they generate [3]. The working principle of the proton exchange membrane (PEM) fuel cell is shown in fig. 1. The polymeric layer must contain adequate moisture for effective proton transfer. The membrane dries out if the cell is run at temperatures outside of its operating range, increasing its ohmic resistance, expansion, and barrier failure. The cell's efficiency deteriorates when the temperature

* Corresponding author, e-mail: dillipkumarsahoo@gmail.com

falls below the operating range, causing water to condense and drift on the cathode surface and lowering the pace of a reaction, voltages, efficiencies, and power production [4]. As a result, changing the temperature of a cell is difficult.

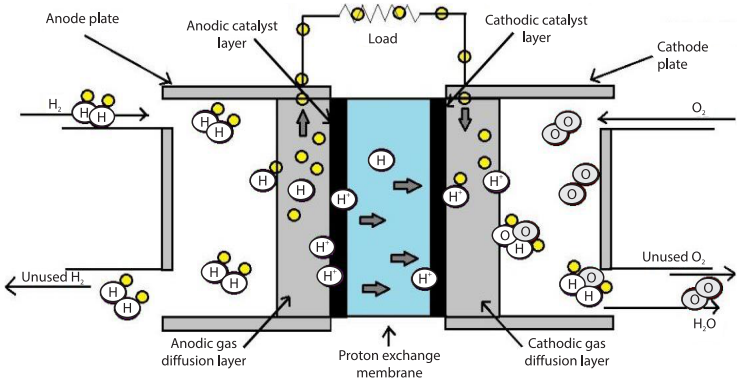

Figure 1. Working Principle of PEM fuel cell

Furthermore, temperature non-uniformity causes the rate of electrochemical processes to fluctuating in various parts of a cell and areas of high spots in certain parts of the cell and a decrease in the cell's lifespan [5]. As a result, temperature field homogeneity must be addressed in addition the cellular temperature limit [6]. The heat generated inside the cell is transferred to the fluid, which cools the cell, and the fluid is then delivered back to a heat exchanger to cool and recirculate inside the cell's mass [7]. In addition the weight of the cell, the system includes a heat exchanger, a water purifier, a pump, and other components. The hot water from the fuel cell enters the radiator, allowing the heat created by the mass fuel to be evacuated with the help of the appropriate fan and the coolant temperature to be decreased to the prescribed level [8]. A controller adjusts the fan speed in this system to keep the temperature of the water entering the cell mass (output from the radiators) at an appropriate processing point. The liquid coolant is divided into two portions after passing through the radiator [9]. A side branch branches out from the main path meets the tank through another branch and then rejoins the main path. The coolant circulates via the pump, increasing the needed water flow and pressure measurement [10]. Because the conductivity of the cooling fluid must be kept to a low at all times, it must pass through an ion exchanger, which separates the ions entering the cooling fluid from the fluid, which is shown as a circuit schematic of a fuel cell cooling system in fig. 2. To examine the influence of temperature on PEM fuel cell performance, [11] a 3-D model provided with a two-phase flow in the gas distribution channel.

A 1-D non-isothermal model was used to investigate the effect of anode and cathode side temperatures on membrane water distribution [12]. The results show that a temperature increase on the anode side can lead to membrane dryness due to considerable electro-osmotic water drag at a high current density. The anode membrane dehydrates when a fuel cell is operated at a high current density [13]. A 3-D numerical model was developed to investigate the impact of various operational variables on the performance of a single PEM fuel cell.

To the best of the author's knowledge, the influence of cooling channel geometry on effective thermal heat transfer and performance in a fuel cell system is still understudied in the literature. This phenomenon is addressed in this study. Numerical modelling is used to explore the geometrical

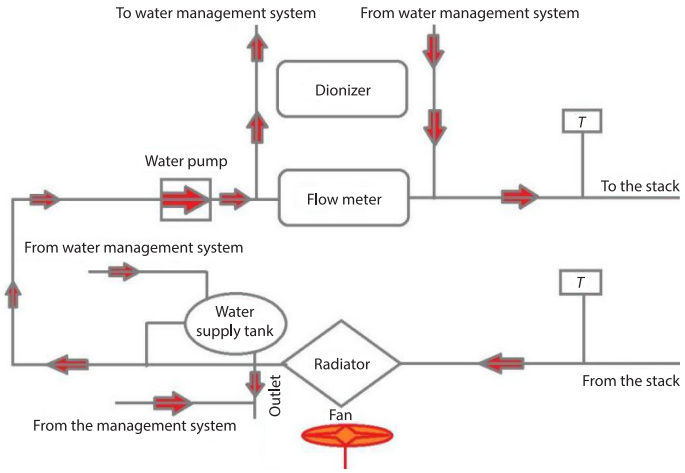

Figure 2. Circuit schematic of a fuel cell cooling system

effect and coolant types on the thermal performance of a PEM fuel cell. In addition, parametric research was undertaken on temperature, relative humidity, and enthalpy on cell performance.

Model description

Numerical research and optimization of geometric parameters of the cooling channel of a PEM fuel cell are carried out using a 3-D entire cell model, and the influence on cell performance is explored. The enthalpy, relative humidity, cell Reynolds number, and internal energy are the critical parameters investigated in this study that influence the fuel cell thermal behavior and subsequent performances. The models of single-cell and stack are shown in fig. 3.

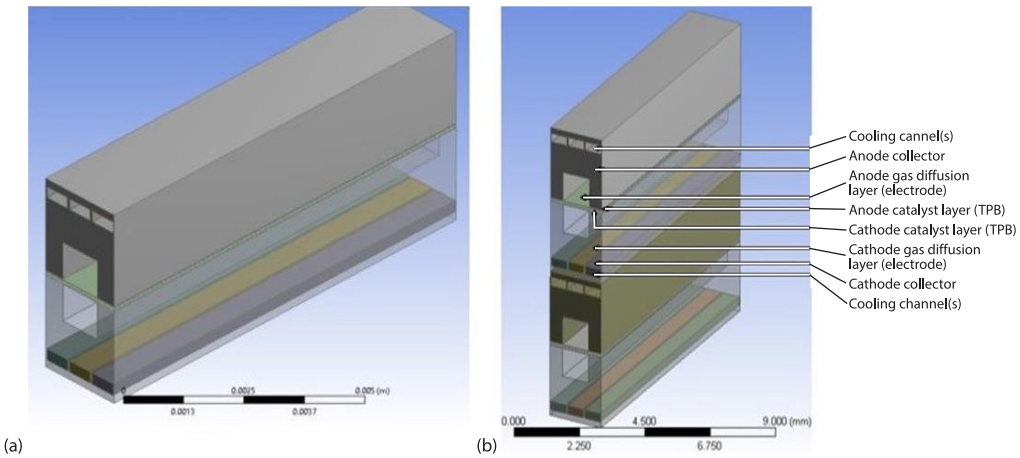

Figure 3. Structure of; (a) single fuel cell and (b) stack

These have been selected as the study's design parameters to be optimized. The construction of three cooling channels transversely organized at similar distances on each side (anode and cathode) of the bipolar plates of the PEM fuel cell is depicted. The remaining physicochemical characteristics of the fuel cell system kept constant in this study are reported in tab. 1, and the properties of the model used are reported in tab. 2.

Table 1. Parameters used in the present model

Geometry	Dimensions
Current collector	2 mm × 2.5 mm × 30 mm
Gas diffusion layer	2 mm × 0.12 mm × 30 mm
Catalyst layer	2 mm × 0.10 mm × 30 mm
Membrane	2 mm × 0.20 mm × 30 mm
Channels	1 mm × 1 mm
Cooling channel	0.25 mm × 0.20 mm

Table 2. Properties used for the present fuel cell model

Descriptions	Single-cell	Stack
Cell operating temperature, [K]	353.15	360
Inlet pressure air/fuel side	3/3	3/3
Operating voltage, [V]	0.65	1.3
Porosity of the gas diffusion layer	0.6	0.6
Absolute permeability of gd layer, [m^2]	$3 \cdot 10^{-12}$	$3 \cdot 10^{-12}$
Porosity of the catalyst layer	0.2	0.2
Absolute permeability of catalyst layer, [m^2]	$2 \cdot 10^{-13}$	$2 \cdot 10^{-13}$
Absolute permeability of membrane, [m^2]	$1 \cdot 10^{-18}$	$1 \cdot 10^{-18}$
Coolant initial temperature, [°]	26.85	26.85
Coolant density, [kgm^{-3}]	998.2	998.2

Coolant description

The DI water is the most often utilized coolant for fuel cell stack cooling. With an electrical resistance of 18 mega ohms, DI water has a high specific heat, thermal conductivity, and viscosity. Therefore, keeping cool with DI water is an excellent idea. The resistivity of DI water, on the other hand, diminishes with time when ions from metals and other sources build. The DI water is also undesirable in colder areas since it freezes at around 0 °C. Therefore, an anti-freezing chemical is added to strengthen the anti-freezing capabilities. Glycol-based mixtures are the most commonly used anti-freezing agents. However, propylene glycol solutions have a higher viscosity and freezing point than ethylene glycol solutions when the two are mixed in the same proportion, making them less thermally efficient, especially at lower temperatures. Consequently, propylene glycol is employed in this study as an anti-freezing agent. The basic properties of the propylene glycol and DI water base are reported in tab. 3.

Table 3. Properties of DI water and propylene glycol

Properties	DI water [100%]	Propylene glycol [100%]
Freezing point, [K]	273	213.15
Boiling point, [K]	373.15	460.16
Density, [gcm^{-3}]	1	1.036
Flashpoint, [K]	not applicable	380.15
Specific heat, [$KJkg^{-1}$]	4.187	2.47
Specific gravity	1.000	1.074

This study makes the coolant by combining propylene glycol (PG) with DI water in four different proportions: DI100, PG10, PG20, and PG30, respectively. The DI100 contains 100% DI water, PG10 contains 90% DI water + 10% PG, PG20 contains 80% DI water + 20% PG, and PG30 contains 70% DI water + 30% PG. Table 4 shows the characteristics of DI water and PG compositions used in this study. The primary goal of this research is to improve process parameters so that the PEM fuel cell system may achieve the best possible implementation in terms of optimal current density under certain operating conditions.

Table 4. Properties of DI water and PG compositions

Properties	PG10	PG20	PG30
Freezing point, [K]	270.15	265.15	287.15
Specific gravity	1.008	1.017	1.026
Boiling point, [K]	372.15	373.70	375.37
Specific heat, [KJkg^{-1}]	4.103	4.021	3.915

Meshing and simulation

The adjoint solver is chosen from ANSYS FLUENT software for meshing the components. An intelligent shape optimization approach uses CFD simulated results to find optimum solutions based on provided objectives and then calculates how to alter the model to achieve the ideal state. First, the flow field and heat transfer model were numerically simulated using the FLUENT programme. Then, the continuity, momentum, and energy equations were solved using finite element techniques.

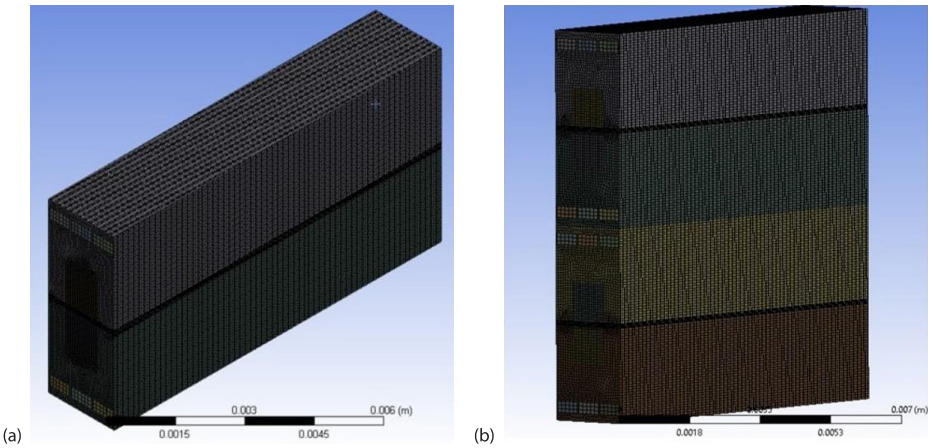

Figure 4. Meshing structure of; (a) single cell and (b) stack

The simple method is used for velocity and pressure coupling, and the second-order upwind technique is assessed for equation discretization. In the mesh with a standard element size, linear element order is applied. To eliminate meshing mistakes in the solution, adaptive scaling is enabled, mesh resolution is set to 7, mesh defeaturing is enabled with standard size with moderate transition, span angle center is fine, skewness is 0.95, and orthogonal value is >1. The single-cell contains 1015596 nodes and 948699 elements shown in fig. 4(a). For stack 607676 nodes and 543712 elements are developed which is shown in fig. 4(b). Series assembled stack is used in this model.

Governing equations

The influential equations are a single set which can be applied to all areas including fluid-flow channels and catalytic layers. This approach is based on the previous work obtained by Obayopo (2018). The following eqs. (1)-(4) are used to determine the mass conservation, mass momentum, species reaction, proton electron and energy reactions happening in fuel cell.

Continuity equation:

$$\nabla\left(\rho i\mathbf{u}\right) = S_m \tag{1}$$

Momentum equation:

$$\frac{1}{\varepsilon^2}\nabla\left(\rho iuu\right) = -\nabla p + \nabla\tau + S_u \tag{2}$$

Species equation:

$$\nabla\left(\mathbf{u}C_k\right) = \nabla\left(D_k^{\text{eff}}\nabla C_k\right) + S_k \tag{3}$$

Energy equation:

$$\nabla\left(\rho ic_p\mathbf{u}T\right) = \nabla\left(k^{\text{eff}}\nabla T\right) + \mathrm{S}_T \tag{4}$$

where ρ_i is the density, $\mathbf{u}$ – the momentum, p – the pressure, Φ_e – the phase potential of the electrolyte membrane, S_m, S_u, S_k are multiple volumetric sources or sinks, η – the over potential, T – the temperature, D_k^{eef} – the diffusion coefficient of species k, C_k – the molar concentration of species k, k^{eef} – the permeability of backing layer, and S_T – the summation of irreversible heat generation and reversible heat release from the fuel cell.

The conservation of mass has been calculated by using the eqs. (5)-(8). The momentum at x-direction was calculated by using eq. (9), similarly the eqs. (9) and (10) are used to find the momentum at y- and z-directions, respectively. The electrochemical reactions occurred at electron and proton side is estimated by using the eqs. (11) and (12), respectively. Similarly the calculation of anode and cathode current transfer densities can be calculated by using Butler Volmer eqs. (13) and (14) [14]:

$$u_v\frac{\partial\left(\rho,y\right)}{\partial x} + v_v\frac{\partial\left(\rho,y\right)}{\partial y} + w_v\frac{\partial\left(\rho,y\right)}{\partial z} = \frac{\partial\left(j_{x,k}\right)}{\partial z} + \frac{\partial\left(j_{y,k}\right)}{\partial y} + \frac{\partial\left(j_{z,k}\right)}{\partial z} + S_k \tag{5}$$

$$S_{\mathrm{H}_2} = -\frac{M_{\mathrm{sH}_2}}{2Fc}R_{\mathrm{an}} \tag{6}$$

$$S_{\mathrm{O}_2} = -\frac{M_{s\mathrm{O}_2}}{2Fc}R_{\mathrm{c}} \tag{7}$$

$$S_{\mathrm{H_2O}} = -\frac{M_{s\ \mathrm{H_2O}}}{2Fc}R_{\mathrm{c}} \tag{8}$$

$$u_v\frac{\partial\left(\rho,u\right)}{\partial x} + v_v\frac{\partial\left(\rho,u\right)}{\partial y} + w_v\frac{\partial\left(\rho,u\right)}{\partial z} = -\frac{\partial p}{\partial x} + \frac{\partial}{\partial x}\left\{\mu_v\frac{\partial u}{\partial x}\right\} + \frac{\partial}{\partial y}\left\{\mu_v\frac{\partial u}{\partial y}\right\} + \frac{\partial}{\partial z}\left\{\mu_v\frac{\partial u}{\partial z}\right\} - \frac{\mu_v u}{\beta_x} \tag{9}$$

$$\nabla e\left(k\nabla eT\right) = -R_{\mathrm{ohm}}I^2 \tag{10}$$

$$\nabla e\left(\sigma_{\text{sol}}\nabla e\varphi_{\text{sol}}\right)+R_{\text{sol}}=0 \tag{11}$$

$$\nabla e\left(\sigma_{\text{mem}}\nabla e\ \varphi_{\text{mem}}\right)+R_{\text{m}}=0 \tag{12}$$

$$R_{\text{an}}=R_{\text{an}}^{\text{ref}}\frac{C_{\text{H}_2}\gamma^{\text{an}}}{C_{\text{H}_2}^{\text{ref}}}\left(e_i^{\frac{\alpha_{\text{anFc}}}{\text{R}T}\eta_{\text{an}}}-e_i^{\frac{-\alpha_{\text{c}}\text{Fc}}{\text{R}T}\eta_{\text{c}}}\right) \tag{13}$$

$$R_{\text{c}}=R_{\text{c}}^{\text{ref}}\frac{C_{\text{O}_2}\gamma^{c}}{C_{\text{O}_2}^{\text{ref}}}\left(e_i^{\frac{-\alpha_{\text{c}}\text{Fc}}{\text{R}T}\eta_{\text{c}}}-e_i^{\frac{\alpha_{\text{anFc}}}{\text{R}T}\eta_{\text{an}}}\right) \tag{14}$$

where u_v, v_v, and w_v [ms^{-1}] are velocity at x-, y-, and z-directions, respectively, ρ_i [kgm^{-3}] – the density of fluid, y_i and $j_{x,k}$, $j_{y,k}$, $j_{z,k}$ are the mass fractions and diffusion mass flux vectors in x-, y-, and z-directions, respectively, S_i [kgs^{-1}m^{-3}] – the mass sink terms and can be found out separately for H_2, O_2, and H_2O separately using eqs. (2)-(4), M_s [kgmol^{-1}] – the molecular weight of different species, and Fc [Cmol^{-1}] – the Faraday's constant, and R_{an} and R_{c} [Am^{-3}] – the exchange current densities at anode and cathode, respectively, which can be found out using eqs. (9) and (10).

Results and discussion

The results were conveniently examined and presented after the simulation analysis was complete. Important factors like curren density, relative humidity, cell Reynolds number, temperature, internal energy, Peclet number, and enthalpy were effectively considered throughout the study.

Analysis of temperature distribution

Figure 5 depicts the PEM fuel cell's temperature effect with an operating temperature range of 300-380 K. Due to the PEM cell's easy accessible in water removal, it was found that its performance was good during the fuel cell temperature range of 357-362 K. As a result, fuel cell flooding caused by water was reduced. The maximum outlet temperatures were 371 K, 365 K, 361 K, and 357 K for DI100, PG10, PG20, and PG30 coolant combinations, respectively, by maintaining a constant fuel cell standard operating temperature of 353.15 K for all coolant conditions. It has been clearly shown that the PG30 coolant combination achieved a lower outlet temperature than other used coolant combinations, indicating that the PG30 combinations have a greater cooling capacity than other used cooant combinations used for this study.

Figure 6 depicts the temperature impact on a PEM fuel cell stack during its operating temperature range of 300-380 K. The simulation results show that the PEM fuel cell efficiency was good when the stack temperature was in the range of 365-368 K because other parameters like relative humidity and enthalpy are optimal during that temperature range. The maximum temperatures of 374K, 368K, 365K, and 356K from DI100, PG10, PG20, and PG30, respectively, were obtained by maintaining the stack standard operating temperature of 360 K for all coolant combinations. It is possible to claim that the PG30 has better cooling capacity than other combinations because it displays a lower outlet temperature than those of other combinations used in this study.

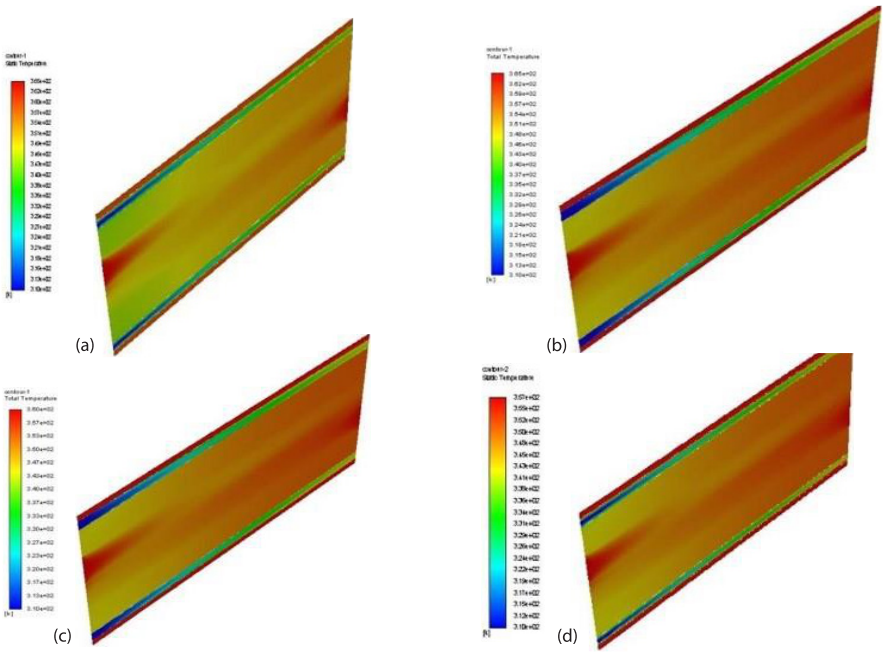

Figure 5. Temperature simulation of single cell fuel cell at different coolant condition of; (a) DI100, (b) PG10, (c) PG20, and (d) PG30

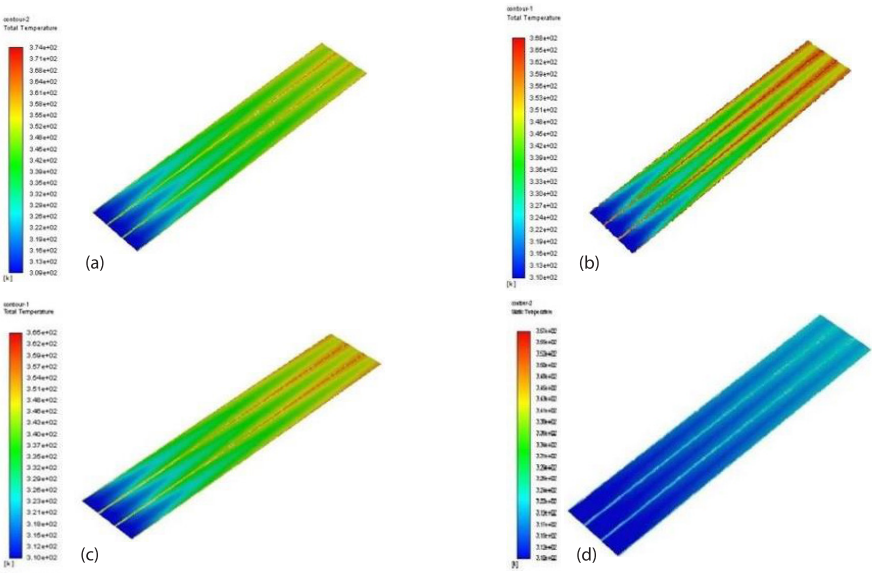

Figure 6. Temperature simulation of fuel cell stack at different coolant condition of; (a) DI100, (b) PG10, (c) PG20, and (d) PG30

Analysis of current density vs. voltage

Figure 7 displays the development of current density for single fuel cells and fuel cell stacks under conditions of standard operating voltage. Figure 7(a) shows the evolution of the current density in a single fuel cell and demonstrates that the current density was highest in the DI100 combination and lowest in the PG30 combination with a fuel cell operating voltage of 0.65 V. The outcome demonstrates that the current density and operating voltage in the DI100 combination had a large gap, whereas in the PG30 combination, the gap was smaller for single cell fuel cells. Figure 7(b) depicts the growth of current density in a fuel cell stack operating at 1.3 V. At PG20 combinations, there was a good correlation between operating voltage and current density, whereas at PG30 combinations, the current density abruptly dropped because of the reduced temperature during that period. The results showed that the PG20 combinations in fuel cell stacks and the PG30 combinations in single cells both show promise for improving fuel cell efficiency.

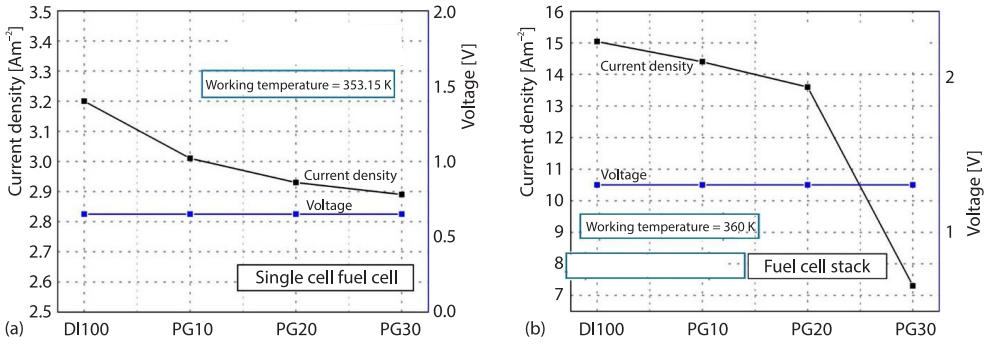

Figure 7. Comparison of current density *vs.* voltage of; (a) single cell fuel cell and (b) fuel cell stack

Analysis of current density vs. Peclet number

Figure 8 shows the thorough examination of current density in relation peclet number for both single fuel cell and fuel cell stack. The ratio of diffusion rate to advective heat transfer is expressed as a dimensionless number called a peclet number. The influence of convective heat transfer will increase as the peclet number rises. In the case of a single cell, refer to fig. 8(a), the peclet number increased gradually from DI100 to PG30 conditions while the current density decreased steadily in the direction of PG30 conditions. The highest peclet number,

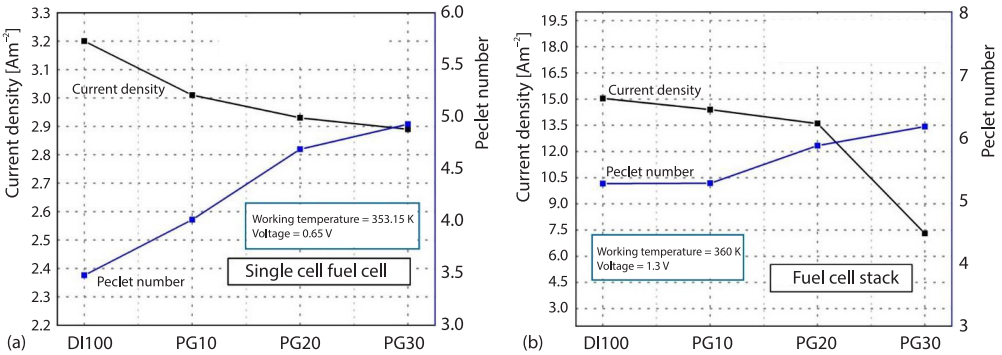

Figure 8. Comparison of current density *vs.* Peclet number of; (a) single cell fuel cell and (b) fuel cell stack

4.9, was observed in a single cell at PG30 combinations. The maximum peclet number of 6.2 was observed for the fuel cell stack, see fig. 8(b), but the current density was low under those circumstances. The PG20 combinations can result in higher efficiency in the case of a fuel cell stack because the PG20 conditions exhibit a good range of Peclet number and current density.

Analysis of membrane water content vs. current density

The relationship between membrane water content and current density for single cell fuel cells and stack fuel cells is shown in fig. 9. The performance and lifespan of the fuel cell are significantly influenced by the amount of water in the membrane. The conductivity of the membrane has a significant impact on the fuel cell's humidity level, so it must be thoroughly dehydrated during operation. Figure 9(a) shows the relationship between the development of water content and current density for a single cell fuel cell, showing that as membrane water content rises, the current density falls. The PG10 condition had a high current density but a low membrane water content, causing the membrane to dry out quickly. However, under PG30 conditions, the fuel cell has a good amount of membrane water relative to the current density, which contributes to improving the fuel cell efficiency. Figure 9(b) illustrates the relationship between membrane water content and current density in the context of a fuel cell stack. Figure 9(b) shows that although the current density in the PG30 condition is very low, the membrane water content is very good, indicating poor fuel cell performance. But in the PG20 condition, an adequate level of membrane water content was present relative to current density, indicating a good performance in the fuel cell stack.

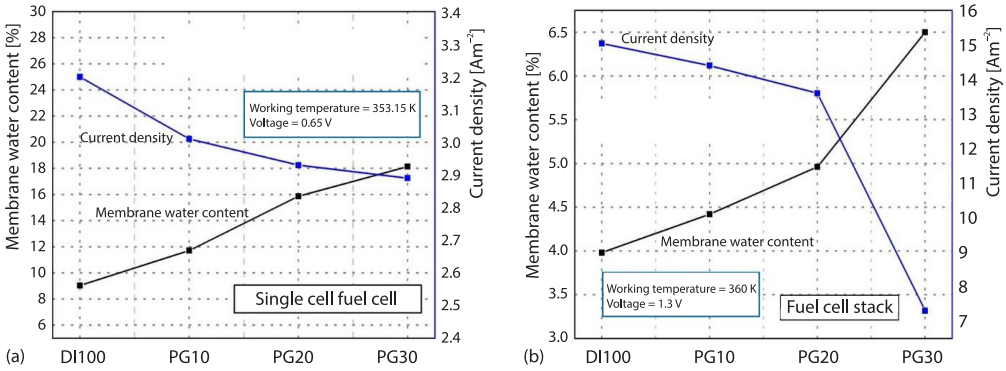

Figure 9. Comparison of membrane water content *vs.* current density at; (a) single cell fuel cell and (b) fuel cell stack.

Analysis of Nusselt number vs. Peclet number

Figure 10 illustrates a thorough investigation of Nusselt number and Peclet number formation in both single-cell fuel cells and fuel cell stacks. The ratio of heat transfer by advection and diffusion in a fuel cell is represented by the Peclet number. A higher Peclet number indicates a stronger convection effect during the transfer of heat and improves the performance of the fuel cell. The Nusselt number provides comprehensive data comparing convection and conduction heat transfer rates. Performance of fuel cells is improved by higher Nusselt numbers. Figure 10(a) shows that the PG30 combinations had the highest Nusselt and Peclet numbers, while the DI100 combinations had the lowest amounts of these numbers. Figure 10(b) illustrates the Nusselt number and Peclet number evolution in the fuel cell stack, confirming

that both numbers are rising from DI100 to PG30 combinations. Very high Nusselt numbers are observed at PG30 combinations, confirming that there is excessive convection heat transfer from the working fluid, which causes a sudden drop in the fuel cell's operating temperature. Figure 10 showed that the PG30 and PG20 coolant mixtures are better suited, for better performance, to single-cell and stack fuel cells, respectively.

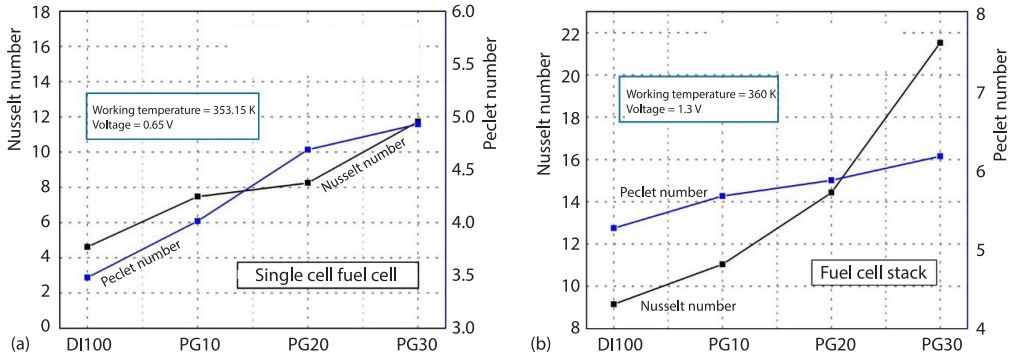

Figure 10. Comparison of current density *vs.* voltage of; (a) single cell fuel cell and (b) fuel cell stack

Analysis of relative humidity vs. temperature

The efficiency and temperature of the fuel cell are significantly influenced by relative humidity. Proton transfer conductivity of the membrane decreases along with a decrease in relative humidity. Generally speaking, low relative humidity can result in decreased electrode kinetics, such as electrode reaction and mass diffusion rates, which can significantly reduce fuel cell performance. For both single cells and fuel cell stacks, fig. 11 shows how relative humidity develops in relation fuel cell outlet temperature. A maximum of 22.3% was observed at the PG30 condition in a single cell, with the relative humidity percentage gradually increasing from the DI100 to PG30 combinations, see fig. 11(a). At PG20 and PG30 combinations, the relative humidity percentage for the fuel cell stack was 14.1%, 23.9%, and the fuel cell temperature was 364.2 K and 357 K, respectively. It has been noted that excessive relative humidity lowers the working temperature and impairs fuel cell performance. Therefore, PG20 combinations are best for improving fuel cell performance.

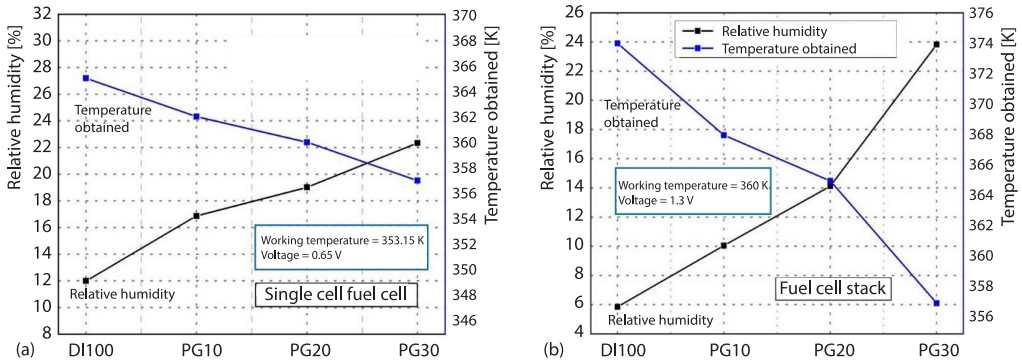

Figure 11. Comparison of relative humidity *vs.* temperature obtained of; (a) single cell fuel cell and (b) fuel cell stack

Analysis of obtained temperature vs. current density

Figure 12 displays the temperature for single cells and fuel cell stacks obtained during operation with respect to current density. The obtained temperature and the current density of the fuel cell have been found to be directly proportional. The temperature of the fuel cell is also reduced as the current density is depleted. In a single-cell fuel cell, fig. 12(a), the obtained temperature and current density are both high under DI100 conditions, whereas PG30 combinations show a lower obtained temperature but acceptable current density. The performance of the fuel cell is impacted by the high obtained temperature's reduction of relative humidity and membrane water content. In the case of the fuel cell stack, fig. 12(b), the temperature and current density were too low under PG30 conditions, whereas PG20 coolant combinations were found to produce an adequate temperature with a good current density and were advised for enhancing fuel cell performance.

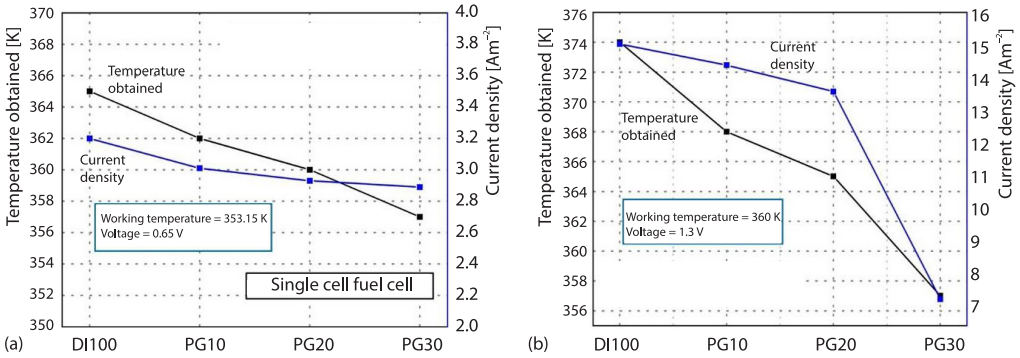

Figure 12. Comparison of temperature obtained *vs.* current density of; (a) single cell fuel cell and (b) fuel cell stack

Analysis of internal energy vs. enthalpy

Figure 13 shows the internal energy and enthalpy formation in a single-cell fuel cell and fuel cell stack. When operating under DI100 conditions, single cell fuel cells have a higher internal energy to enthalpy formation ratio than when operating under PG30 combinations, see fig. 13(a). Fuel cells perform better when the internal energy to enthalpy ratio is lower, so PG30 is suggested for single cell fuel cells. In the case of a fuel cell stack, both the DI100 and PG30 combinations have the lowest internal energy to enthalpy ratios, refer fig. 13(b). However, the

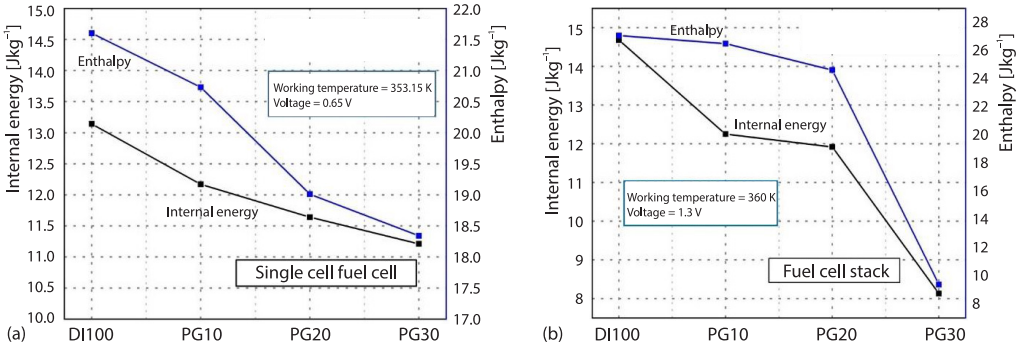

Figure 13. Comparison of Internal energy *vs.* enthalpy of; (a) single cell fuel cell and (b) fuel cell stack

ratio value in PG30 combinations is lower than the DI100 value. In light of this, DI100 combinations are appropriate for fuel cell stacks when internal energy and enthalpy formation are issues.

Conclusions

This research intends to build a cooling system to increase fuel cell performance at high operating temperatures by integrating operational factors with various coolants and cooling channel designs. Operating factors such as relative humidity, Peclet number, membrane water content, and temperature, according to numerical calculations, have a significant influence on fuel cell performance. The optimal temperature, relative humidity, and membrane water content values for several coolants were determined using an optimiser's straightforward problem adjoint solution. Fuel cell productivity significantly increases when research factors are merged for the unique PEM fuel cell model working conditions tested in this study, are as follows.

- First, the functionality is satisfactory at 356 K, attained with the PG30 requirement for a single cell. Then, the performance improvement steadily decreased from 362 K to 371 K, as measured by the PG10 and PG20 conditions. It should be highlighted that beyond 371 K because the membrane is dehydrated, no significant improvement in cell function can be expected.
- Similarly, the fuel cell functioning is good at a temperature of 365 K, which is produced using the PG20 condition in fuel cell stack. After then, the performance increase began to wane progressively, starting at 368 K with the PG10 condition. It's worth noting that the temperature attained with the PG30 condition is 357 k, which is lower than the working temperature, resulting in cell flooding. This study may simply be broadened to incorporate alternative coolants in PEM stack systems to increase PEM fuel cell performance.

References

[1] Alshorman., A., Design and Investigation of Optimum Cooling System for Operative Performance of PEM Fuel Cell, *International Journal of Emerging Trends in Engineering and Development*, *8* (2018), 1, pp. 32-43
[2] Xing., Y., *et al.*, Temperature Control for a Proton-Exchange Membrane Fuel Cell System with Unknown Dynamic Compensations, *Complexity*, *2020* (2020), ID8822835
[3] Asghari, S., *et al*., Design of Thermal Management Subsystem for A 5 kW Polymer Electrolyte Membrane Fuel Cell System, *Journal Power Sources*, *196* (2011), 6, 3141
[4] Li, Q., *et al*., A Review on Temperature Control of Proton Exchange Membrane Fuel Cells, *Processes*, *9* (2021), 235
[5] Afshari E., *et al*., Analyses of Heat and Water Transport Interactions in A Proton Exchange Membrane Fuel Cell, *Journal Power Sources*, *194* (2006), 423
[6] Wang., Y., *et al*., Thermal Management System Modelling and Simulation of a Full-Powered Fuel Cell Vehicle, *Journal Energy Resour. Technol*., *142* (2020), 6, 061304, JERT-19-1468
[7] Rahgoshay., S. M., *et al*., Thermal Investigation of a Pem Fuel Cell with Cooling Flow Field, *Energy*, 134 (2017), 1, pp. 61-73
[8] Zhang, G., Kandlikar, S. G., A Critical Review Of Cooling Techniques In Proton Exchange Membrane Fuel Cell Stacks, *Int. J. Hydrogen Energy*, 37 (2012), 2412
[9] Baharlou Houreh, N., *et al*., The 3-D CFD Modelling of a Planar Membrane Humidity for Pem Fuel Cell Systems, *Int. J. Hydrogen Energy*, *39* (2014), 14969
[10] Maharudrayya, S., *et al*., Pressure Drops and Flow Distribution in Multiple Parallel-Channel Configurations Used in Proton Exchange Membrane Fuel Cell Stacks, *Journal of Power Sources*, *157* (2006), 1, pp. 358-367
[11] Coppo, M., *et al*., On the Influence of Temperature on Pem Fuel Cell Operation, *Journal of Power Sources*, *159* (2006), 1, pp. 560-569

[12] Yan, W.-M., *et al*., Analysis of Thermal and Water Management with Temperature-Dependent Diffusion Effects in the Membrane of Proton Exchange Membrane Fuel Cell, *Journal of Power Sources*, *129* (2004), 2, pp. 127-137
[13] Obayopo, S. O., *et al*., The 3-D Optimization of a Fuel Gas Channel of a Pem Fuel Cell For Maximum Current Density, *International Journal of Energy Research*, *37* (2013), 3, pp. 228-241
[14] Praveenkumar, S., *et al.*, Influence of Pressure and Temperature on the Performance of Pem Fuel Cell with Taper Flow Channel Design, *International Journal of Applied Chemistry*, *11* (2015), 4, pp. 505-513

Paper submitted: April 29, 2022
Paper revised: November 10, 20222
Paper accepted: December 17, 2022